EMAS
Engineering Modelling, Analysis & Simulation
THE NAFEMS JOURNAL

NAFEMS
Vol. 4, Issue 1, 2027

Computationally Efficient Modelling of Induction-based Preheating of Wire Feedstock for Additive Manufacturing

Ruofeng Cao, Yongle Sun[1], Wojciech Suder, Stewart Williams

Welding and Additive Manufacturing Centre, Cranfield University, Bedfordshire, MK43 0AL, UK

Abstract

Wire-based directed energy deposition (DED) additive manufacturing (AM) uses an intense energy source to melt metal wire feedstock and is capable of efficiently depositing large-scale components. Wire preheating is promising to enhance the DED process productivity and part quality. Induction heating (IH) is a controllable non-contact method for rapidly and precisely preheating the wire feedstock, thereby significantly increasing the deposition rate. However, IH-based preheating of moving wire feedstock is complicated and underexplored for AM applications. In this study, to understand the complex electromagnetic heating mechanism, a multiphysics finite element model of coupled electromagnetic and thermal fields was developed based on the formulation in Eulerian frame, which improves the computational efficiency by 80.9 % compared to the model in Lagrangian frame. Furthermore, in the case of wire feedstock passing through a stationary magnetic field at a constant feed speed, a more efficient steady-state approach was proposed with 98.9 % computational time saving than the transient model. The temperature prediction by the model was validated by thermocouple measurement in an experiment. A range of coil geometries and setups were evaluated using the developed efficient model, revealing the coil effects on the wire preheating temperature and energy transfer.

Keywords

Induction preheating, Additive manufacturing, Directed energy deposition, Lagrangian method, Eulerian method

1 Introduction

Feedstock preheating is an auxiliary process in wire-based directed energy deposition (DED) additive manufacturing (AM) to increase deposition rate or mitigate the undesirable effects caused by the intense heat input during deposition of large-scale metal parts. As a result of the wire preheating, the energy required from the primary heat source (e.g. electric arc, electron beam and laser) to form the deposit bead is reduced, which is beneficial for minimising remelting and suppressing large epitaxial columnar grain growth during the layer-by-layer deposition [1]. Previous research has demonstrated that hot wire also mitigates the porosity through cleaning the wire surface, which reduces the formation of trapped gas pores, removes contaminants such as oxygen, carbon and silicon, and changes the behaviour of hydrogen in the melt pool [2], [3], [4]. In addition, wire preheating is an effective strategy to increase deposition rates significantly, since for given power capacity and limit of the primary heat source a higher wire feed speed can be applied after wire preheating [5], [6], and it also improves energy absorption of wire in laser DED AM [7], [8], [9].

Conventional preheating techniques directly involve the Joule effect, such as resistance heating and bypass heating, which generate an electric current through an additional cable connected to an auxiliary

[1]Corresponding author.
E-mail address: Yongle.Sun@cranfield.ac.uk (Yongle Sun)
https://doi.org/10.59972/9hu7g7ag

power source. However, the disadvantage of these techniques is the loss of stability of the arc for AM due to the induced magnetic blow, and consequently it limits the flexibility for wire feeding. Induction heating (IH) is an effective non-contact heating method, offering a highly controllable heat source suitable for rapid preheating, which avoids magnetic blow and is applicable to most metals [10], [11]. During IH-based wire preheating, the wire moves through and is exposed to a high frequency alternating magnetic field, which generates eddy currents inside the material, resulting in precise heating of the moving feedstock to the target temperature due to the material resistance. Electromagnetic and heat transfer phenomena are involved in IH, which are complex physical processes; hitherto, inductive preheating of moving feedstock is an underexplored research area for AM. The existent studies usually used the coil current input, instead of the actual preheating temperature in the wire, to indicate the degree of wire preheating. In this context, there is a gap in accurately controlling the preheating temperature and optimising the IH process for AM.

The present study is aimed to understand the electromagnetic heating phenomena during IH-based wire feedstock preheating via evaluation of various coil geometries and setups using a highly efficient multiphysics model and investigating their effects on preheating temperature and energy transfer. A 2D axisymmetric finite element model is developed to couple the electromagnetic and thermal fields, enabling the study of the temperature evolution of a moving metal wire passing through a high-frequency magnetic field using models in both Lagrangian and Eulerian frames. The proposed numerical model can accurately predict the transient temperature profile of the moving wire. Additionally, the steady-state model can significantly improve the computational efficiency.

2 Material and Methods

A 2D axisymmetric finite element model was generated to couple the electromagnetic and thermal fields. The computational domain encompasses the wire, coil, and air, as illustrated in Figure 1.a-b. for the Lagrangian frame and c-d. for the Eulerian frame. The following assumptions or simplifications are made to reduce the complexity of the modelling.

- The air domain is limited to the region surrounding the coil and the wire. The contribution of the far field to the induction heating is assumed to be negligible, as the electromagnetic field intensity decays with distance from the coil [12].
- An infinite element domain is introduced at the outer boundary of the air domain to model an open space. This artificial domain prevents field distortion at the air boundary, and such distortion introduces errors in the electromagnetic field [9].
- The coil is assumed to be a toroid without winding structure. This simplification preserves the essential current distribution and magnetic field generation while significantly reducing the complexity and allowing 2D representation [13].
- The computational domain is divided into several physical-field domains in which the equations are not all solved. The electromagnetic field is solved in the infinite element domain, the air domain, the wire domain, and the coil domain, while the thermal field is solved only in the wire domain.

The wire passes through the coil at a constant feed speed during the IH-based wire preheating. The temperature profile is not only related to the position of the wire in the magnetic field but also to the thermal history of the heated wire. The model created in this study uses Lagrangian and Eulerian frames to describe the dynamic thermal effects of the moving wire. In the Lagrangian frame, the material coordinate system moves with the wire, and the mesh is updated over time. Notably, a part of the air domain needs to be defined to move synchronously with the wire domain, forming a moving computational subdomain associated with the wire motion. Local mesh refinement was applied in the moving air boundaries based on the minimum time step to mitigate excessive mesh distortion induced by the mesh motion [14]. The moving air domain does not represent physical air motion; it is introduced to facilitate the Lagrangian description of the moving wire. An identical continuity boundary condition was imposed at the interface between the moving air subdomain and the stationary air domain to ensure continuity of the magnetic field and magnetic flux across the boundary, as shown in Figure 1.a. Differently, the modelling domain in the Eulerian frame is unchanged throughout the simulation, as shown in Figure 1.c. The field variables are expressed as functions of fixed coordinates in the spatial coordinate system and the model updates the state of the domain at each time step based on a fixed mesh without domain motion. Specifically, it should be noted that in the Lagrangian frame the length of the wire and the air domain with synchronous motion was adopted to be 270 mm, as compared to the

150 mm wire length considered in the Eulerian frame. The larger wire length in the Lagrangian model is necessary to obtain results equivalent to the Eulerian model at the same heating time, and a moving mesh method was employed to simulate the actual motion trajectory of the wire. Furthermore, extending the air domain to the full length of the wire would introduce a large number of elements in regions where the magnetic field has already decayed to negligible levels in the Lagrangian frame. Therefore, the air domain was deliberately reduced, such that further enlargement of the air domain provided no additional contribution to the preheating temperature, ensuring comparable numerical accuracy between the models in the Lagrangian and Eulerian frames.

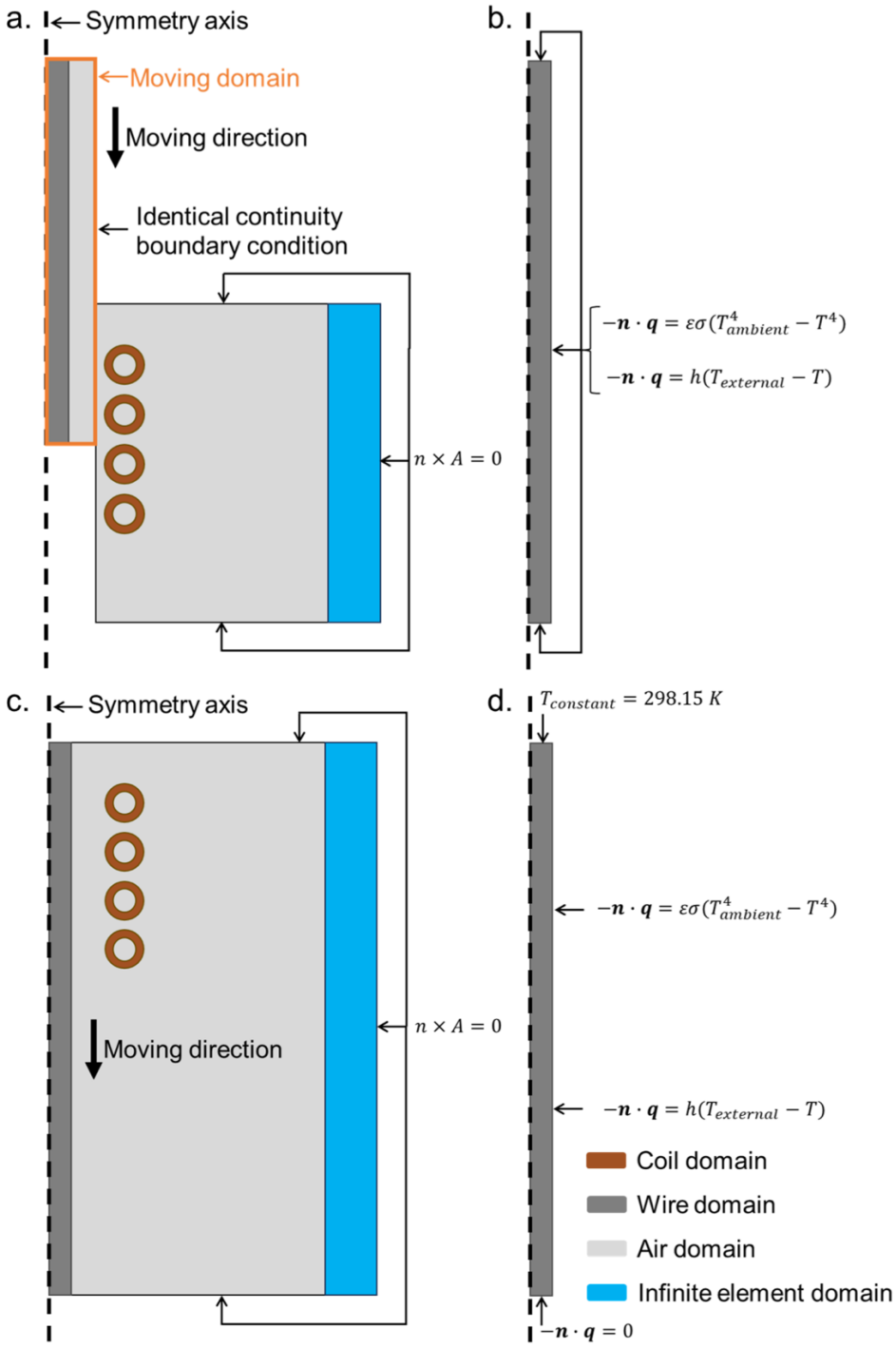

Figure 1. Illustration of computational domains and boundary conditions: a. Electromagnetic field in Lagrangian frame, b. Thermal field in Lagrangian frame, c. Electromagnetic field in Eulerian frame, d. Thermal field in Eulerian frame.

The IH process parameters are summarised in Table 1. A stainless-steel filler wire, typically used in wire-based DED AM, was considered in the model, and its chemical composition is provided in Table 2. The relative magnetic permeability [15], [16], electrical conductivity, thermal conductivity and constant-pressure specific heat capacity of the wire were adopted from the literature [9].

Table 1. Geometrical and IH parameters of the finite element model.

Geometrical / IH parameter	Value
Wire diameter	1.6 mm
Wire length	150 mm (Eulerian frame) 270 mm (Lagrangian frame)
Wire feed speed	5 mm/s
Coil turns	7
Distance between adjacent turns	1 mm
Coil length	41 mm
Coupling distance	6.7 mm
Current	300 A
Frequency	355 kHz
Heating time	20 s

Table 2. Chemical composition of the stainless-steel wire (unit: wt%).

C	Cr	Ni	Mo	Mn	Si	P	S	Cu	Fe
0.07	18.6	8.0	1.2	7.1	0.8	0.03	0.03	0.75	Balance

The boundary conditions of the models in the Lagrangian and Eulerian frames are same in the electromagnetic fields (Figure 1.a and c.) The description of the electromagnetic field in each computational domain is derived from Maxwell equations [17]. By introducing the magnetic vector potential $\vec{A}$, the governing equations for the electromagnetic field analysis are Eq. (1) - Eq. (7). The initial condition of the magnetic field is $\vec{A} = 0$, and the magnetic insulation boundary condition is set at the boundary of the air domain.

Air domain:

$$\nabla \times \frac{1}{\mu} \nabla \times \vec{A} - \nabla \times \left(\frac{1}{\mu} \nabla \cdot \vec{A} \right) = 0 \tag{1}$$

$$\vec{j} = 0 \tag{2}$$

Coil domain:

$$\overrightarrow{J_s} = \nabla \times \frac{1}{\mu} \nabla \times \vec{A} - \nabla \times \left(\frac{1}{\mu} \nabla \cdot \vec{A} \right) \tag{3}$$

$$\vec{j} = \overrightarrow{J_s} \tag{4}$$

Wire domain:

$$\nabla^2 \varphi + \frac{\partial (\nabla \cdot \vec{A})}{\partial t} = 0 \tag{5}$$

$$\nabla \times \frac{1}{\mu} \nabla \times \vec{A} - \nabla \times \left(\frac{1}{\mu} \nabla \cdot \vec{A} \right) + \frac{\partial \vec{A}}{\partial t} + \sigma \nabla \varphi = 0 \tag{6}$$

$$\overrightarrow{J_e} = \frac{\partial \vec{A}}{\partial t} - \sigma \nabla \varphi \tag{7}$$

where $\vec{j}$ is the current density (A/m^2), $\overrightarrow{J_e}$ is the eddy current density (A/m^2), $\overrightarrow{J_s}$ is the source current density (A/m^2) in the coil, μ is the magnetic permeability (H/m), $\vec{A}$ is the magnetic vector potential (Wb/m), φ is the scalar potential (V), and σ is the electrical conductivity (S/m).

The water-cooling channel inside the coil of the IH system ensures no substantial variation in the coil temperature. Therefore, for the thermal field, only the wire domain is considered, as shown in Figure 1.b. and Figure 1. d. The heat conduction within the wire domain is described by Eq. (8) in the transient model. The Eq. (9) is the governing equation of the steady-state model.

$$\rho C_p \frac{\partial T}{\partial t} + \rho C_p u \cdot \nabla T - \nabla \cdot (k \nabla T) = Q_e = Q_{rh} + Q_{ml} \tag{8}$$

$$\rho C_p u \cdot \nabla T - \nabla \cdot (k \nabla T) = Q_e = Q_{rh} + Q_{ml} \tag{9}$$

$$Q_{rh} = \frac{1}{2} Re(J \cdot E^*) \tag{10}$$

$$Q_{ml} = \frac{1}{2} Re(j\omega B \cdot H^*) \tag{11}$$

where ρ is the density (kg/m^3), C_p is the specific heat capacity (J/(kg·K)), u is the feed speed of the moving wire (m/s), ∇T is the temperature gradient (K/m), k is the thermal conductivity (W/(m·K)), Q_{rh} is the resistive loss of eddy current (W/m^3), Q_{ml} is the magnetic loss (hysteresis) (W/m^3), Re is the real part of the product $J \cdot E^*$, j is the imaginary unit, and ω is the angular frequency (rad/s).

The boundary conditions of the thermal field are determined by convection (Eq. (12)) and radiation (Eq. (13)) in the Lagrangian frame. In the Eulerian frame, the two cross-sectional ends of the wire are the modelling boundaries of the computational domain of the wire rather than the actual wire ends. Therefore, a constant temperature equal to the room temperature was set at the inlet end, indicating the temperature of the wire before entering the coil, and the thermal insulation boundary condition was set at the outlet end to represent the internal cross-section of the wire without convection and radiation.

$$-n \cdot q = h(T_{external} - T) \tag{12}$$

$$-n \cdot q = \varepsilon\sigma(T_{ambient}^4 - T^4) \tag{13}$$

where q is heat flux (W/m^2), $h = 15$ W/(m^2·K) is convection coefficient, $T_{external}$ is external environment temperature (304.15 K), $\varepsilon = 0.5$ is emissivity of wire surface, σ is Stefan-Boltzmann constant (5.670374419×10^{-8} W/(m^2·K^4)), and $T_{ambient}$ is ambient temperature (304.15 K).

Figure 2 shows the meshes of the two finite element models. Due to the skin depth, a fine boundary layer mesh was added to the wire and coil. The air domain also has a fine mesh to resolve the magnetic field around the coil. A coarse mesh was used for the rest. The finite element model was solved using a high-performance workstation with AMD Ryzen Threadripper PRO 5945WX CPU (12 cores). The MUMPS solver in COMSOL software was employed in conjunction with linear finite element interpolation to ensure numerical stability and robustness. Temporal discretisation was carried out using the implicit backward Euler method, with the maximum step size constrained to be 0.01 seconds.

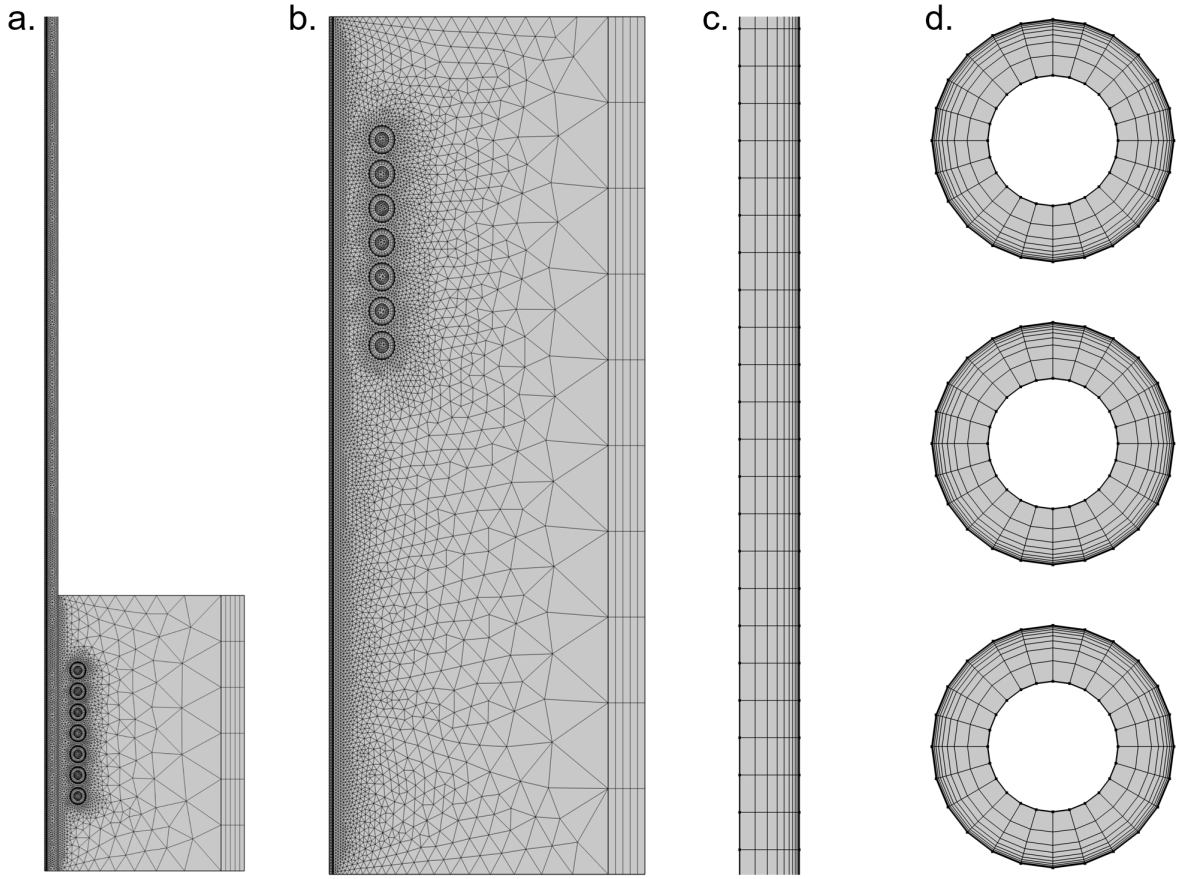

Figure 2. Meshes in the finite element models: a. Lagrangian model, b. Eulerian model; and the zoomed-in view of the boundary layer mesh: c. Wire, d. Coil. The scale ratio is 1.8 (Lagrangian model):1 (Eulerian model).

3 Results and Discussion

3.1 Experimental validation

A moving wire induction heating experiment was conducted to validate the transient models using the Lagrangian and Eulerian approaches (the experimental parameters are also provided in Table 1). As shown in Figure 3.a, the experimental setup was same as that used in the authors' previous work [9], consisting of a K-type thermocouple, a fixture, a 7-turn helical coil, and an induction heating system (Ambrell EASYHEAT). The coil was operated at a current of 300 A. The wire was fed at a speed of 10 mm/s by a wire feeder and passed through a straightener before entering the coil. The thermocouple was positioned 50 mm away from the coil to monitor the wire surface temperature while avoiding interference from the magnetic field. A flexible spring was used to maintain stable contact between the thermocouple and the wire surface without disturbing the wire motion. The simulation results are in good agreement with experimental measurement (Figure 3.b), especially for the temperature at the stable level under a quasi-steady state. The predicted temperatures by the Lagrangian and Eulerian models are also consistent, with only 0.18 % difference.

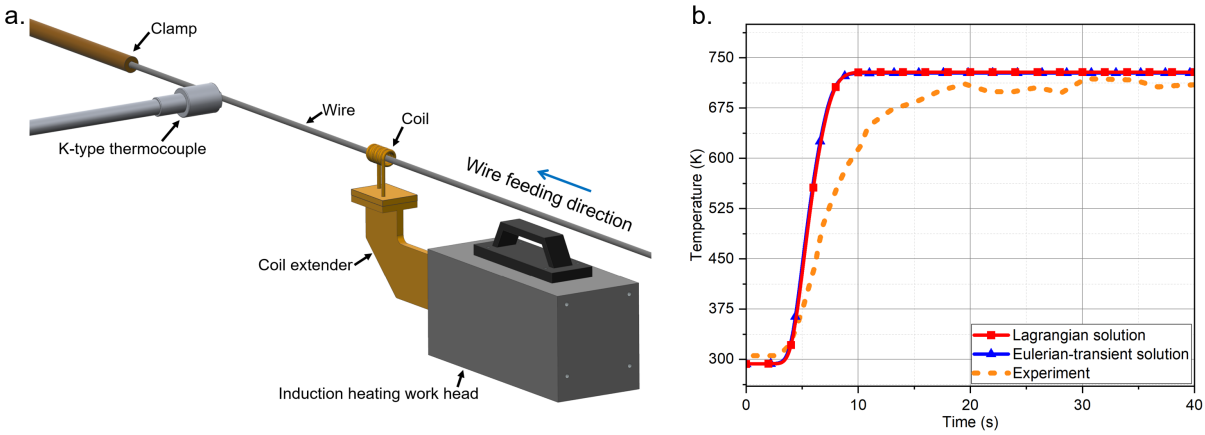

Figure 3.a. Schematic of experimental setup, b. Comparison between experimental and transient modelling results.

3.2 Comparison between different simulation techniques

The prediction differences in temperature and magnetic field intensity between the Lagrangian and Eulerian transient models are less than 1 %, particularly small after the wire attains the quasi-steady state (Figure 4). Table 3 shows the numbers of elements in the models and the comparison of the computational time. The computational time for the Eulerian transient model is significantly reduced by 80.9%.

Table 3. Comparison between the Lagrangian and Eulerian transient models.

	Number of elements	Computational time	Time saving by Eulerian model
Lagrangian model	14272	5030 s	N/A
Eulerian model	14109	963 s	80.9 %

3.3 Applicability of the steady-state model

Both the prediction by the transient model and the experimental result (section 3.1) indicate that the wire temperature attained a steady-state stage after heating of short time, and the temperature distribution in the space tends to be constant. It is hence surmised that each section of the wire experiences the same thermal cycle after it passes through the coil and then loses heat by convection and radiation to the environment, gradually reaching a thermal equilibrium in the space. In a wire-based DED AM process, constant wire preheating temperature is essential for melt pool stability and deposition quality. A steady-state model was hence created in the Eulerian frame described using the spatial coordinate system. Figure 5 shows the surface temperature distribution of the wire. It is evident that the temperature fields predicted by the steady-state and transient models are almost identical. However, the computational time of the steady-state model is only 11 seconds, meaning that the total time saving is around 98.9 % in comparison with the Eulerian transient model.

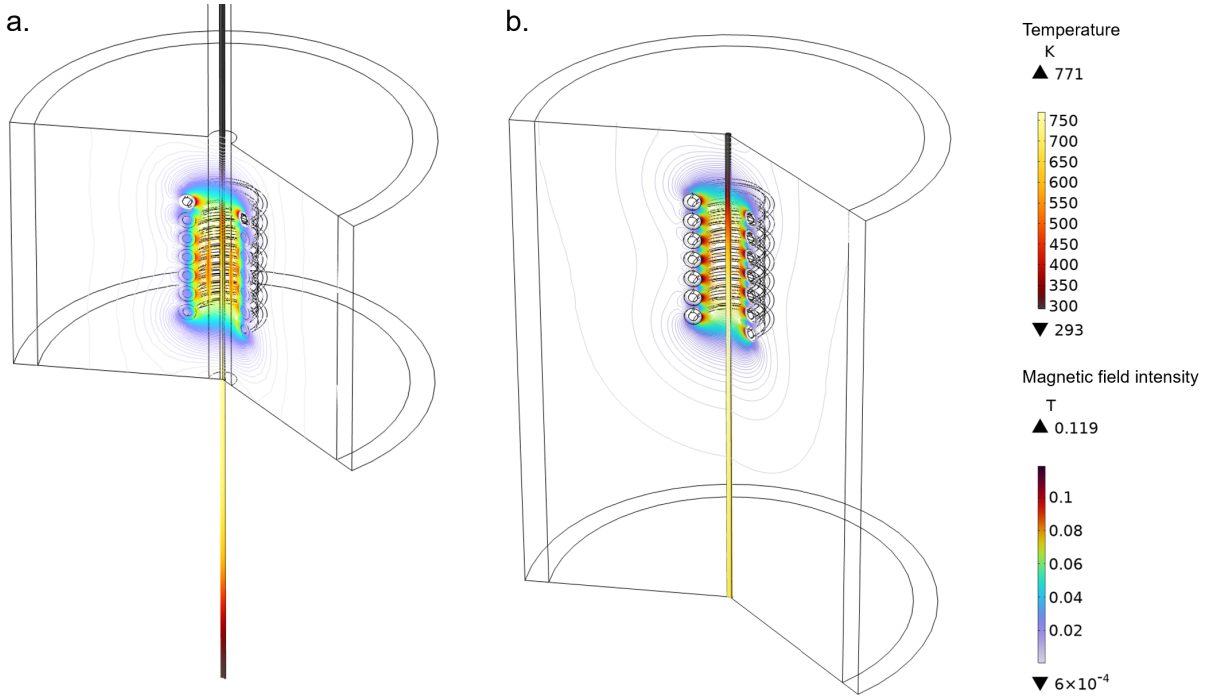

Figure 4. Distributions of temperature (unit: K) in the wire and magnetic field intensity (unit: T) in the air: a. Lagrangian transient model, b. Eulerian transient model.

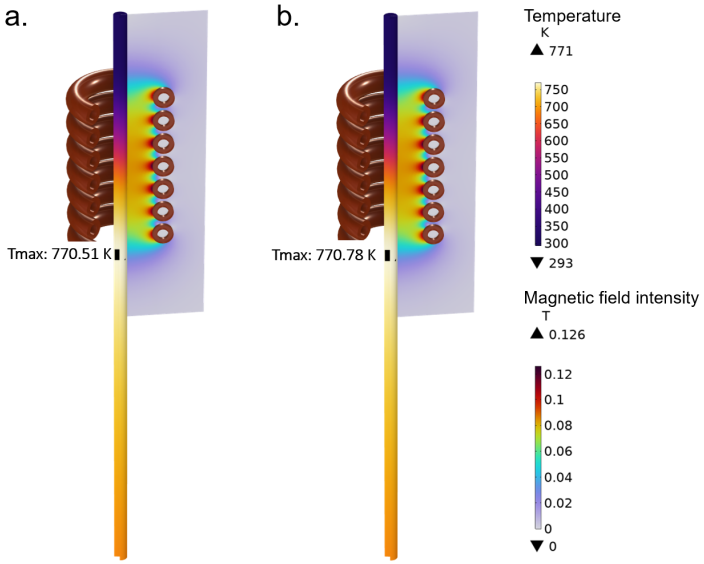

Figure 5. Thermal and magnetic profiles predicted by the models in the Eulerian frame (the wire diameter is exaggerated by two times): a. Steady-state model, b. Transient model (t = 20 s).

3.4 Influence of coil geometry on wire preheating

Due to the high computational efficiency, the Eulerian steady-state model was employed to further analyse the effects of different coil geometries (Figure 6) on wire preheating. Figure 7 shows the temperature distributions on the wire surface in the steady state for the helical and spiral coils. The wire temperature rose rapidly after entering the coil area and reached the highest temperature at the exit end of the coil, and then the wire temperature exhibited an approximately linear decrease. The wire temperature profiles for the helical coils with different section shapes are almost the same, while the wire achieves a higher temperature in the spiral coil. It is hence demonstrated that the coil shape influences the wire preheating temperature, which, however, is insensitive to the coil wire cross-section. The smaller distance between the spiral coil and the wire allows the magnetic field to have a higher

coupling efficiency. Therefore, the coil geometry should be appropriately adjusted to obtain the desired preheating temperature.

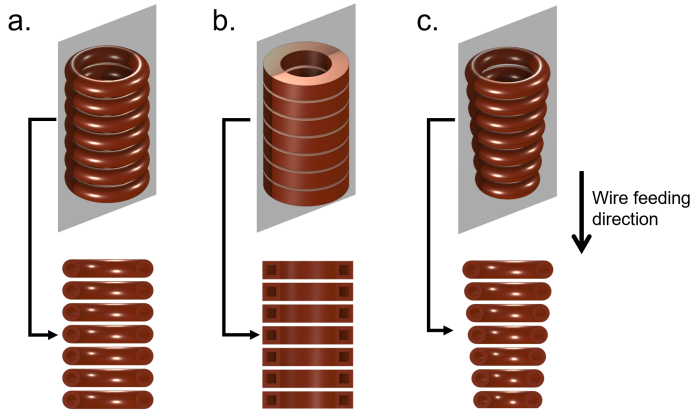

Figure 6.a. Helical coil with circular section (this coil was used in the validation experiment), b. Helical coil with rectangular section, and c. Spiral coil with circular section.

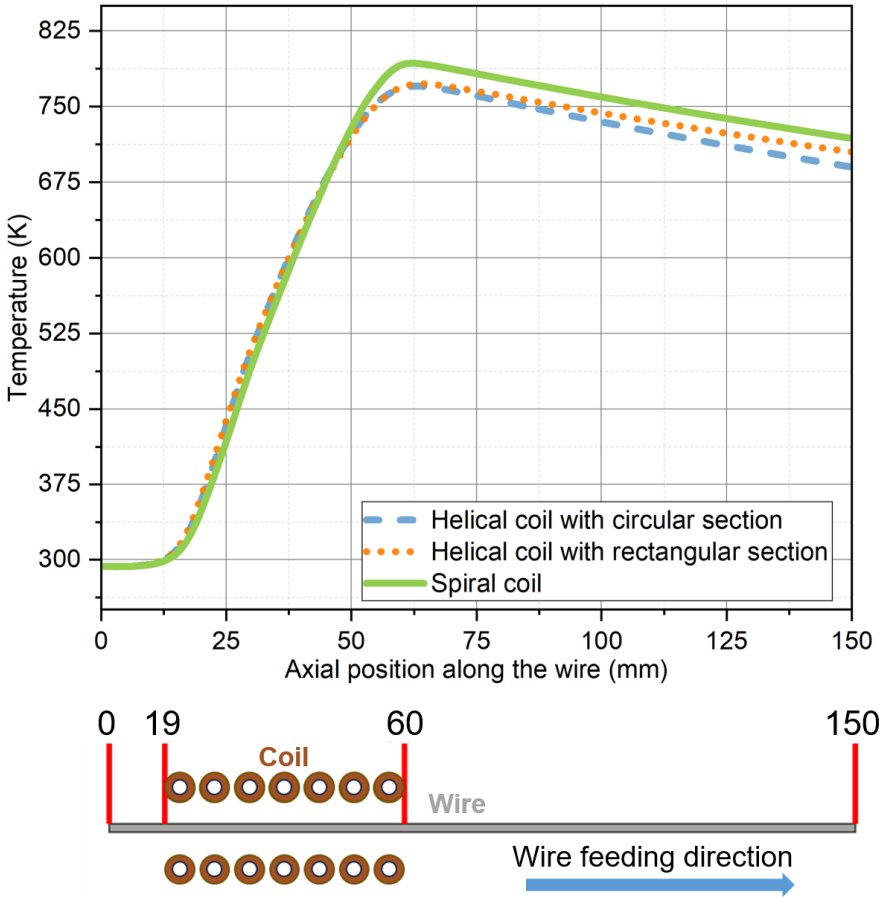

Figure 7. The temperature distribution on the wire surface in the computational domain.

3.5 Coil with magnetic concentrator

To further explore a better heating strategy, a Ferrotron 559H magnetic concentrator was added around the helical coil. The material parameters of the magnetic concentrator were adopted from the literature [18]. Figure 8 shows the temperature and magnetic flux density slices of the wire. It is seen that the concentrator plays an important role in the magnetic field distribution. Compared with the helical coil alone, the coil with the magnetic concentrator increased the peak temperature from 770.78 K to 805.13 K. Through volume integration in the wire domain using the electromagnetic volume loss density, it is

found that the energy transferred to the wire increased from 43.68 W to 46.56 W after adding the magnetic concentrator. This would be useful for future work where the magnetic concentrator can be optimised to maximise the energy transfer to the wire.

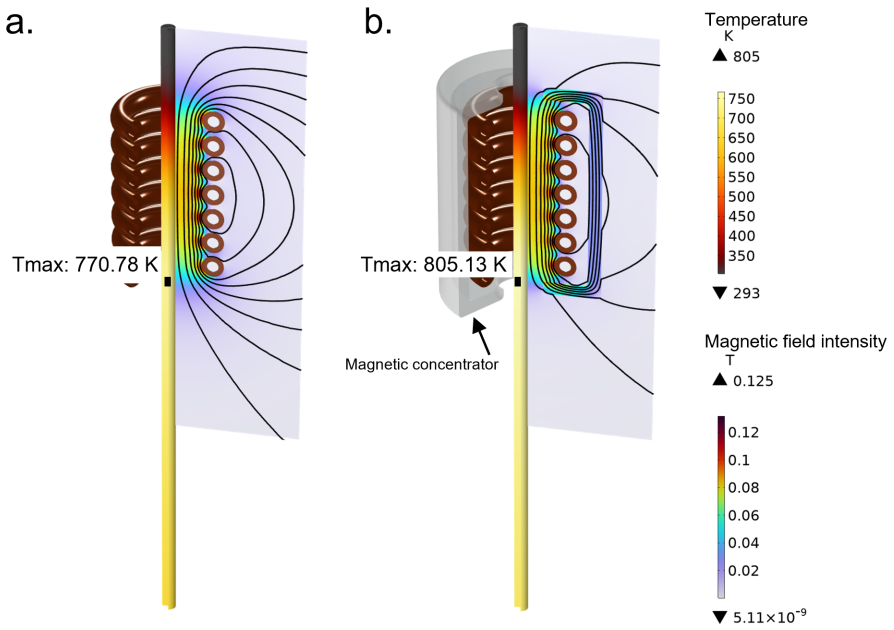

Figure 8. Temperature profile in the wire domain and magnetic field strength in the air domain under steady state (the wire diameter is exaggerated by two times): a. Helical coil alone, and b. Helical coil with magnetic concentrator.

4 Conclusions

This study developed electromagnetic and thermal coupling models based on the Lagrangian and Eulerian frames to analyse the induction-based preheating of a moving filler wire for DED AM. The model prediction was validated by the experiment, and different simulation methods were compared. The following conclusions are drawn:

- Both the Lagrangian and Eulerian transient models accurately predict the evolution of the wire preheating temperature. The Lagrangian model replicates the real-world motion of the wire, while the Eulerian model focuses on the physical variables in a controlled volume and shows an 80.9 % saving in computational time for a similar prediction accuracy.
- The Eulerian steady-state model is applicable to the induction heating problem of the moving wire after reaching thermal equilibrium in the controlled volume, showing a significant advantage of 98.9 % computational time saving compared to the Eulerian transient model.
- The modified coil geometry and the addition of a magnetic concentrator can improve the wire preheating performance, a result that is beneficial for enhancing heating uniformity and energy efficiency. The developed Eulerian transient and steady-state models can be used in further study of the interaction between wire preheating and deposition in wire-based DED AM for process optimisation.

5 Acknowledgement

Ruofeng Cao would like to thank Sonia Martins Meco, Nisar Shah, Ryan Cafferty and Mark Allen for their technical support. The authors also would like to thank Landing Gear Industrial Breakthroughs (I-Break) programme for the financial support (Project Ref. 10003486 funded by Aerospace Technology Institute, Innovate UK).

6 References

[1] T. Xu, M. Zhang, J. Wang, T. Lu, S. Ma, and C. Liu, 'Research on high efficiency deposition method of titanium alloy based on double-hot-wire arc additive manufacturing and heat treatment', *J. Manuf. Process.*, vol. 79, pp. 60–69, 2022, doi: https://doi.org/10.1016/j.jmapro.2022.04.044.

[2] T. Lu *et al.*, 'Hot-wire arc additive manufacturing Ti–6.5Al–2Zr–1Mo–1V titanium alloy: Pore characterization, microstructural evolution, and mechanical properties', *J. Alloys Compd.*, vol. 817, p. 153334, 2020, doi: https://doi.org/10.1016/j.jallcom.2019.153334.

[3] J. Gu, M. Gao, S. Yang, J. Bai, J. Ding, and X. Fang, 'Pore formation and evolution in wire + arc additively manufactured 2319 Al alloy', *Addit. Manuf.*, vol. 30, p. 100900, 2019, doi: https://doi.org/10.1016/j.addma.2019.100900.

[4] E. M. Ryan, T. J. Sabin, J. F. Watts, and M. J. Whiting, 'The influence of build parameters and wire batch on porosity of wire and arc additive manufactured aluminium alloy 2319', *J. Mater. Process. Technol.*, vol. 262, pp. 577–584, 2018, doi: https://doi.org/10.1016/j.jmatprotec.2018.07.030.

[5] H. Mao *et al.*, 'Improve the manufacturing efficiency of steel bars by using hot-wire pulse arc additive manufacturing', *J. Manuf. Process.*, vol. 89, pp. 430–443, 2023, doi: https://doi.org/10.1016/j.jmapro.2023.01.074.

[6] P. Poolperm, W. Nakkiew, and N. Naksuk, 'Experimental Investigation of Additive Manufacturing Using a Hot-Wire Plasma Welding Process on Titanium Parts', *Materials*, vol. 14, no. 5, 2021, doi: 10.3390/ma14051270.

[7] A. Kisielewicz *et al.*, 'Hot-Wire Laser-Directed Energy Deposition: Process Characteristics and Benefits of Resistive Pre-Heating of the Feedstock Wire', *Metals (Basel).*, vol. 11, no. 4, 2021, doi: 10.3390/met11040634.

[8] R. H. Phillips and E. A. Metzbower, 'Laser beam welding of HY80 and HY100 steels using hot welding wire addition', *WELDING JOURNAL-NEW YORK-*, vol. 71, pp. 201-s, 1992.

[9] R. Cao, Y. Sun, W. Suder, X. Chen, Z. Li, and S. Williams, 'Modelling and analysis of induction preheating of moving filler wire for directed energy deposition', *Int. J. Heat Mass Transf.*, vol. 257, p. 128192, 2026, doi: https://doi.org/10.1016/j.ijheatmasstransfer.2025.128192.

[10] C. Jing *et al.*, 'Improving mechanical strength and isotropy for wire-arc additive manufactured 304L stainless steels via controlling arc heat input', *Materials Science and Engineering: A*, vol. 845, p. 143223, 2022, doi: https://doi.org/10.1016/j.msea.2022.143223.

[11] A. L. Voigt, T. V. da Cunha, and C. E. Niño, 'Conception, implementation and evaluation of induction wire heating system applied to hot wire GTAW (IHW-GTAW)', *J. Mater. Process. Technol.*, vol. 281, p. 116615, 2020.

[12] V. Rudnev, D. Loveless, R. L. Cook, and M. Black, *Handbook of Induction Heating*. 2002. doi: 10.1201/9781420028904.

[13] A. K. Prasad, S. Kapil, and S. Bag, 'Critical conditions for melting of metallic wire in induction heating system through numerical simulation and experiments', *J. Manuf. Process.*, vol. 77, pp. 678–693, 2022, doi: https://doi.org/10.1016/j.jmapro.2022.03.054.

[14] W. Huang, Y. Ren, and R. D. Russell, 'Moving Mesh Methods Based on Moving Mesh Partial Differential Equations', *J. Comput. Phys.*, vol. 113, no. 2, pp. 279–290, 1994, doi: https://doi.org/10.1006/jcph.1994.1135.

[15] R. Sukhon, R. Kongchana, K. Khongsiri, B. Puntaratronnugoon, and V. Tulasombut, 'A study on volumetric magnetic susceptibility of weight due to its manufacturing process', in *Proceedings of the IMEKO*, 2010.

[16] A. Suprihanto, 'Magnetic properties of austenitic stainless steel 316l and 316lvm after high temperature gas nitriding treatment', *ROTASI*, vol. 19, no. 2, pp. 72–75, 2017.

[17] X. Zhang, C. Chen, and Y. Liu, 'Numerical analysis and experimental research of triangle induction heating of the rolled plate', *Proc. Inst. Mech. Eng. C J. Mech. Eng. Sci.*, vol. 231, no. 5, pp. 844–859, 2017.

[18] V. Nemkov, R. Ruffini, and A. Kolesnichenko, 'Composite Materials for Magnetic Field Control in EPM', in *International Symp. on Heating by EM Sources, Padua*, pp. 19–22.